Miniaturized selective plane illumination microscopy for high-contrast *in vivo* fluorescence imaging

Christoph J. Engelbrecht,† Fabian Voigt,† and Fritjof Helmchen*

Department of Neurophysiology, Brain Research Institute, University of Zurich, Winterthurerstrasse 190, CH-8057 Zurich, Switzerland

**Corresponding author: helmchen@hifo.uzh.ch*

Received December 3, 2009; revised February 17, 2010; accepted March 8, 2010; posted March 10, 2010 (Doc. ID 120738); published April 28, 2010

Light-sheet-based fluorescence imaging techniques rely on simultaneous excitation of a single optical plane and thus permit high-contrast optically sectioned imaging of extended tissue samples. Here, we introduce a miniaturized fiber-optic implementation of a selective plane-illumination microscope (miniSPIM). The excitation light was delivered through a single-mode optical fiber, and a light-sheet was created with a cylindrical gradient-index lens and a right-angle microprism. Fluorescence emission was collected orthogonally to the light-sheet through a gradient-index lens assembly and a coherent fiber bundle. The end face of the fiber bundle was imaged onto a charge-coupled device camera. The spatial resolutions of the miniSPIM were 3.2 μm laterally and 5.1 μm axially. Images of fluorescent beads and neurons in mouse neocortex exhibited superior axial resolution and contrast in the miniSPIM-mode compared to images recorded in epi-illumination mode. The miniSPIM may thus enable novel *in vivo* imaging approaches.

OCIS codes: 110.2945, 170.0180, 170.2520, 170.3880, 180.2520.

Technological advances of miniature fiber-optic imaging devices open promising avenues for biomedical research and clinical imaging. Various approaches have been explored to build miniature high-resolution fluorescence microscopes (reviewed in [1]). Major goals are endoscopic cellular imaging in hardly accessible tissues such as deep brain regions as well as imaging with portable devices [2–5], for example, in order to measure neural activities in freely behaving animals [4,5].

Two fundamentally different fluorescence excitation modes are usually employed. First, point-scanning nonlinear techniques like two-photon microscopy exhibit intrinsic optical sectioning and low susceptibility to scattering [6]. They suffer, however, from high costs and mechanical complexity and are limited in temporal resolution. In contrast, epi-fluorescence wide-field technologies that are based on single-photon excitation provide faster parallel recording schemes using cameras. Nonetheless, they lack optical sectioning capability and suffer from high fluorescence background and strong light scattering in turbid media.

Light-sheet-based microscopy combines advantages of both approaches: intrinsic optical sectioning and wide-field image acquisition (reviewed in [7]). Implementations are based on sheet-like illumination through a low-NA excitation light path, which is rotated by 90° with respect to the optical axis of the high-NA detection objective lens. Fluorescence excitation is confined to the focal plane of the detection objective lens, thus minimizing the out-of-focus fluorescence background. Light-sheet illumination results in excellent three-dimensional resolution [8], high-contrast imaging, parallel camera-based image acquisition, and decreased photodamage [7]. A first approach to shrink the size of a light-sheet-based microscope using gradient-index (GRIN) lenses for fluorescence excitation has been reported [9], but an overall miniaturization with potential applications for *in vivo* brain imaging or clinical endoscopy is still pending.

Here, we present a miniaturized fiber-optic implementation of a selective plane-illumination microscope (miniSPIM) that is based on custom 1 mm diameter GRIN lenses (GRINTECH) for light-sheet creation and fluorescence detection. In addition to the miniSPIM-mode we implemented an epi-illumination-mode for comparison.

The experimental setup is shown in Fig. 1. The proximal optical system consisted of a laser for fluorescence excitation, a tunable beam splitter setup, beam shaping and coupling optics, and a microscope setup for fluorescence emission detection [Fig. 1(a)]. Vertically polarized laser light (488 nm, 5–75 mW, Coherent Sapphire) was distributed between the miniSPIM- and epi-excitation beam paths via a combination of an achromatic half-wave plate ($\lambda/2$, AHWP05M-630, Thorlabs) and a polarizing beam splitter cube (NT49-002, Edmund Optics). In the miniSPIM-path, the laser light was coupled into a single-mode fiber (SMF, S460, Thorlabs) via a fiber port (PAF-X-5-A, Thorlabs) and then guided to the miniSPIM front piece for light-sheet creation. In the epi-excitation beam path, the laser beam was first expanded by a Galilean telescope and subsequently focused into the backfocal plane of the objective lens (OL, Fluar 10×/0.5, Zeiss) via a projection lens L3 and a dichroic mirror (DCM, BS R488, AHF Analysentechnik). The laser light was coupled into a coherent fiber bundle (CFB, IGN-08/30, 30,000 cores, 4 μm core spacing, Sumitomo Electric Industries) in front of the OL. In both excitation modes, fluorescence emission was collected through the CFB. The proxi-

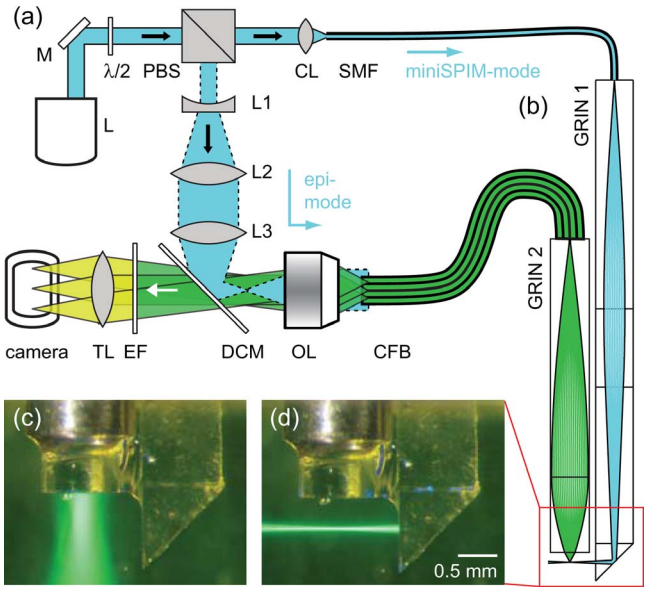

Fig. 1. (Color online) miniSPIM. (a) Proximal optical system consisting of L, laser; M, mirror; λ/2, half-wave plate; PBS, polarizing beam splitter cube; CL, fiber coupling lens; L1 and L2, Galileo telescope; L3, projection lens; DCM, dichroic mirror; OL, objective lens; EF, emission filter; TL, tube lens; and camera. SMF and CFB connect the proximal optical system (a) to the miniaturized miniSPIM front piece (b). The front piece consists of two GRIN-assemblies, GRIN 1 and GRIN 2. (c) and (d) Photographs of the front part of the front piece taken in fluorescein solution to visualize (c) epi-excitation and (d) miniSPIM-excitation modes.

mal end of the fiber bundle was imaged onto a camera (pco.2000, pco AG) via a wide-field microscope setup consisting of OL, DCM, emission filter (EF, Razoredge LP 514, Semrock), and tube lens (TL, 452960, Zeiss). The EF was selected to block autofluorescence from the fiber bundle.

The miniSPIM front piece consisted of two adjacent GRIN-lens assemblies with a total weight of less than 1.5 g [Fig. 1(b)]. The miniSPIM-excitation assembly GRIN 1 consisted of a rotationally symmetric collimator lens (NA 0.11) at the distal end of the SMF, a cylindrical GRIN lens for light-sheet generation (design NA of 0.06), a glass spacer, and a microprism deflector. The light-sheet thickness was measured by direct imaging of the light-sheet onto a camera. FWHMs were 4.6 μm in the center and 6.7 μm at the edges of the detection field of view ($\approx$300 μm diameter). The objective assembly GRIN 2 for epi-illumination and fluorescence collection consisted of two rotationally symmetric GRIN lenses with NAs of 0.2 for CFB-coupling and 0.5 for imaging (magnification of 2.5×, working distance of 0.3 mm in water). While illumination in epi-mode (excitation and detection both through CFB and GRIN 2) caused fluorescence excitation in a large cone in front of GRIN 2 [Fig. 1(c)], illumination in miniSPIM-mode (excitation through SMF and GRIN 1; detection through GRIN 2 and CFB) excited fluorescence only in a light sheet that coincides with the focal plane of GRIN 2 [Fig. 1(d)], thus enabling intrinsic optical sectioning.

To quantify the lateral and axial resolutions of the miniSPIM and to assess contrast, we imaged 1 μm diameter fluorescent microspheres (Fluoresbrite YG, 17154, Polysciences) embedded in 1% agarose gel. The miniSPIM front piece was attached to a three-axis micromanipulator and two separate image stacks ($\Delta z = 1$ μm) were acquired for the epi- and miniSPIM-modes by moving the head piece with respect to the sample. Image stacks were rescaled to isotropic voxel size using ImageJ. Gaussian blurring with two-pixel radius ($\approx$1.5 μm) was applied to the raw xy images for smoothed visualization and analysis. Line intensity profiles through individual beads were measured both laterally and axially in the xy and xz planes with highest maximum intensities and were fitted with Gaussian curves (Fig. 2). The lateral resolution was not significantly different for the miniSPIM- and epi-modes (3.2±0.4 and 3.3±0.4 μm FWHM, respectively; mean±standard deviation; $n = 10$ beads; $P > 0.7$, unpaired two-tailed t-test). These experimental values corresponded well to the expected resolution of 3.2 μm, which was limited by undersampling in the CFB (calculated from $2d/M$, core spacing of $d = 4$ μm, and GRIN 2 magnification of $M = 2.5\times$). The axial resolution was significantly improved in the miniSPIM-mode (5.1±1.0 and 11.5±2.3 μm FWHM for miniSPIM-mode versus epi-mode, $P \ll 0.0001$). This result directly demonstrates the superior optical sectioning capability of the miniSPIM-mode. Moreover, the contrast of bead images [calculated as $C = (I_{max} - I_{min})/(I_{max} + I_{min})$] was significantly larger in the miniSPIM-mode ($C = 0.69 \pm 0.05$) compared to the epi-mode ($C = 0.27 \pm 0.07$, $P \ll 0.0001$).

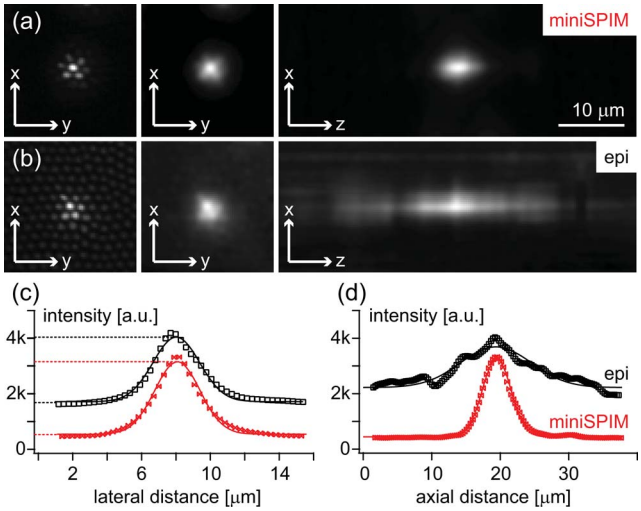

Fig. 2. (Color online) Characterization of miniSPIM. (a) 1 μm fluorescent microspheres were used to quantify lateral and axial miniSPIM-resolutions. Left column, raw pixelated xy image. Center column, depixelated xy image using a Gaussian blur filter. Right column, xz projection after isotropic rescaling. (b) 1 μm fluorescent microsphere imaged in epi-mode. Same columns as above. All images are maximum intensity projections and were brightness/contrast adjusted. (c) Line profiles through depixelated xy images of beads and Gaussian fits for miniSPIM- (red) and epi- (black) modes. Maximum and minimum intensity values are indicated. (d) Axial profiles through beads with Gaussian fits for miniSPIM-(red) and epi- (black) modes.

We applied the miniSPIM to image GABAergic interneurons from transgenic GAD67-GFP mice [10] in paraformaldehyde-fixed brain tissue and *in vivo*. Animal procedures were approved by the Cantonal Veterinary Office, Zurich. For fixed tissue experiments, 4-mm-thick coronal brain slices were cut and mounted in an upright position with agarose gel [Fig. 3(a)]. Subsequently, z stacks with a spacing of $\Delta z = 2.5$ μm were acquired as described above. At an imaging depth of $z \approx 230$ μm, cells were hardly discernible in the epi-mode because of the weak contrast and high fluorescence background, whereas they were still clearly visible in the miniSPIM-mode [Fig. 3(b)]. As judged from the image contrast, the low-NA excitation light-sheet was not substantially degraded by scattering if the path length inside the sample was kept short (≈400 μm). To limit this path length in *in vivo* experiments, an additional spacer (thickness of 500 μm, $n = 1.33$, MY-133 UV-curable adhesive, MY Polymers) was attached to the face of the microprism. For *in vivo* imaging, we performed a craniotomy to allow access to the cortex of urethane-anesthetized mice. Subsequently, the dura was carefully removed and a 1 mm wedge of brain tissue was surgically excised for the insertion of the miniSPIM microprism and spacer [Fig. 3(c)]. Similar to our results from fixed tissue, imaging in the epi-mode was limited by a strong fluorescence background, whereas the miniSPIM-excitation enabled cell discrimination at $z \approx 125$ μm depth [Fig. 3(d)]. These results demonstrate the benefits of the miniSPIM instrument for imaging in strongly scattering biological tissues.

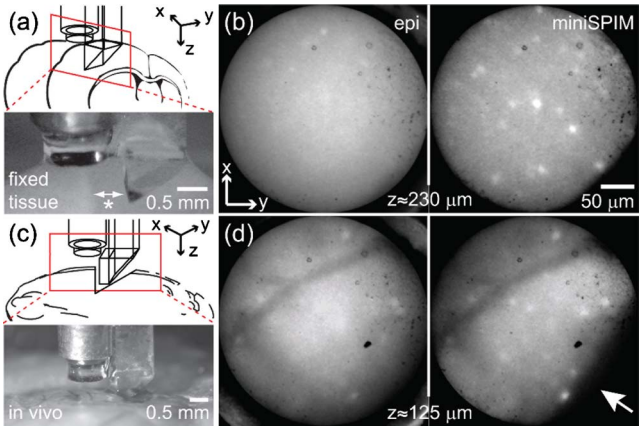

Fig. 3. (Color online) Application of miniSPIM to image GFP-expressing interneurons in fixed tissue (top row) and *in vivo* (bottom row). (a) Experimental setup for imaging in fixed mouse neocortex. Arrow (with asterisk) indicates the distance between microprism face and tissue edge. (b) Images acquired at a depth of $z \approx 230$ μm below the brain surface. Left: epi-mode; right: miniSPIM-mode. (c) *In vivo* imaging setup with spacer. (d) *In vivo* images acquired at a depth of $z \approx 125$ μm in epi- (left) and miniSPIM- (right) modes. All images are single planes from z-stacks and were brightness/contrast adjusted. Incoming light-sheet direction for miniSPIM-mode is indicated by an arrow.

In summary, we have introduced a fully miniaturized implementation of a light sheet based microscope. We characterized the spatial resolution and contrast and found significant improvements compared to epi-wide-field illumination. The lateral resolution was limited by the core spacing of the CFB, resulting in a lower spatial resolution compared to non-miniaturized SPIM [8]. However, the CFB may be unnecessary for stationary imaging, in which case the backfocal plane of the GRIN 2 could be directly imaged. On the other hand, fiber-optic implementations have promising applications in neuroscience, e.g., calcium imaging of neuronal population activity in freely behaving animals [4,5]. Depending on the target area, microprism-insertion into the tissue may be unavoidable [11]. The use of a custom blunt prism and a possible size reduction of the front piece may help to minimize invasiveness and keep light paths short. In addition, the use of near-IR excitable dyes [12] could alleviate scattering of the excitation light-sheet and emitted fluorescence photons and thus further increase the contrast and imaging depth in strongly scattering biological tissues.

The authors thank H.-J. Kasper and S. Giger for expert technical assistance, K. Schulz and D. Langer for help with biological preparations, and K. Vogt for the GAD67-GFP knock-in mouse line, originally made by Y. Yanagawa. This work was supported by the National Center of Competence in Research "Neural Plasticity and Repair" and by grants from the Swiss National Science Foundation (3100A0-114624), the EU-FP7 program (200873), and the Swiss SystemsX.ch initiative (Neurochoice project).

†Both authors contributed equally to this research.

References

1. B. A. Flusberg, E. D. Cocker, W. Piyawattanametha, J. C. Jung, E. L. M. Cheung, and M. J. Schnitzer, Nat. Methods **2**, 941 (2005).
2. F. Helmchen, M. S. Fee, D. W. Tank, and W. Denk, Neuron **31**, 903 (2001).
3. C. J. Engelbrecht, R. S. Johnston, E. J. Seibel, and F. Helmchen, Opt. Express **16**, 5556 (2008).
4. B. A. Flusberg, A. Nimmerjahn, E. D. Cocker, E. A. Mukamel, R. P. J. Barretto, T. H. Ko, L. D. Burns, J. C. Jung, and M. J. Schnitzer, Nat. Methods **5**, 935 (2008).
5. J. Sawinski, D. J. Wallace, D. S. Greenberg, S. Grossmann, W. Denk, and J. N. D. Kerr, Proc. Natl. Acad. Sci. USA **106**, 19557 (2009).
6. F. Helmchen and W. Denk, Nat. Methods **2**, 932 (2005).
7. J. Huisken and D. Y. R. Stainier, Development **136**, 1963 (2009).
8. C. J. Engelbrecht and E. H. Stelzer, Opt. Lett. **31**, 1477 (2006).
9. D. Turaga and T. E. Holy, Opt. Lett. **33**, 2302 (2008).
10. N. Tamamaki, Y. Yanagawa, R. Tomioka, J.-I. Miyazaki, K. Obata, and T. Kaneko, J. Comp. Neurol. **467**, 60 (2003).
11. T. H. Chia and M. J. Levene, J. Neurophysiol. **102**, 1310 (2009).
12. X. Shu, A. Royant, M. Z. Lin, T. A. Aguilera, V. Lev-Ram, P. A. Steinbach, and R. Y. Tsien, Science **324**, 804 (2009).